The Binding and Release of Oxygen and Hydrogen Peroxide Are Directed by a Hydrophobic Tunnel in Cholesterol Oxidase[†]

Lin Chen,[‡] Artem Y. Lyubimov,[§] Leighanne Brammer,[§] Alice Vrielink,[§,||] and Nicole S. Sampson*[,‡]

Department of Chemistry, Stony Brook University, Stony Brook, New York 11794, Department of Biology and Chemistry, University of California, Sinsheimer Labs, 1156 High Street, Santa Cruz, California 95064, and School of Biomedical Biomolecular and Chemical Sciences, University of Western Australia, 35 Stirling Highway, Crawley, WA 6009, Australia

Received February 7, 2008; Revised Manuscript Received March 18, 2008

ABSTRACT: The usage by enzymes of specific binding pathways for gaseous substrates or products is debated. The crystal structure of the redox enzyme cholesterol oxidase, determined at sub-angstrom resolution, revealed a hydrophobic tunnel that may serve as a binding pathway for oxygen and hydrogen peroxide. This tunnel is formed by a cascade of conformational rearrangements and connects the active site with the exterior surface of the protein. To elucidate the relationship between this tunnel and gas binding and release, three mutant enzymes were constructed to block the tunnel or its putative gate. Mutation of the proposed gating residue Asn485 to Asp or tunnel residue Phe359 or Gly347 to Trp or Asn reduces the catalytic efficiency of oxidation. The K_{mO_2} increases from 300 ± 35 μM for the wild-type enzyme to 617 ± 15 μM for the F359W mutant. The k_{cat} for the F359W mutant-catalyzed reaction decreases 13-fold relative to that of the wild-type-catalyzed reaction. The N485D and G347N mutants could not be saturated with oxygen. Transfer of hydride from the sterol to the flavin prosthetic group is no longer rate-limiting for these tunnel mutants. The steady-state kinetics of both wild-type and tunnel mutant enzymes are consistent with formation of a ternary complex of steroid and oxygen during catalysis. Furthermore, kinetic cooperativity with respect to molecular oxygen is observed with the tunnel mutants, but not with the wild-type enzyme. A rate-limiting conformational change for binding and release of oxygen and hydrogen peroxide, respectively, is consistent with the cooperative kinetics. In the atomic-resolution structure of F359W, the indole ring of the tryptophan completely fills the tunnel and is observed in only a single conformation. The size of the indole is proposed to limit conformational rearrangement of residue 359 that leads to tunnel opening in the wild-type enzyme. Overall, these results substantiate the functional importance of the tunnel for substrate binding and product release.

Enzymes often catalyze reactions in which one or more of the substrates are gases, for example, small diatomic molecules like oxygen or hydrogen. Due to the small, nonpolar nature of these molecules, the requirements for their specific binding have long been debated. It is possible that these gases may reach the active sites of enzymes by passive diffusion through proteins as they undergo "breathing" vibrations. The passive diffusion of small gases could occur along many different trajectories through a protein. However, there are many atomic-resolution structures of enzymes and proteins in which possible binding cavities and even tunnels have been observed. In some cases, these tunnels have been saturated with xenon, an efficient diffractor of X-rays, to demonstrate that a gas may diffuse through a channel or tunnel (*1*−*4*). Here, we present functional evidence that the observed hydrophobic tunnel in type I cholesterol oxidase is required for efficient gas binding and release.

Enzymes that channel an intermediate between two active sites are the best characterized examples of functional tunnels (*5*). These tunnels sequester a gaseous or reactive intermediate that is generated at one active site and direct its diffusion to a second active site. For example, tryptophan synthase channels indole generated in one subunit to the adjacent subunit where it is converted to tryptophan (*6*). Members of the amidotransferase family, of which carbamoyl phosphate synthetase is an exemplary member, channel ammonia produced from substrate, e.g., glutamine, from one active site to a second where the ammonia is utilized in a second reaction. In the case of carbamoyl phosphate synthetases, carbamate is subsequently channeled to a third active site (*7*−*9*). 4-Hydroxy-2-ketovalerate aldolase/aldehyde dehydrogenase (acylating) channels a toxic acetaldehyde intermediate between two distant active sites located 25 Å from each other as a means of protecting the cell from the adverse effects of the intermediate before it is converted to acetyl-coenzyme A (*10*). In these examples, blocking diffusion of an intermediate into bulk solution and the ensuing improvement in catalytic efficiency are the primary mechanistic advantages that result from tunneling of metabolites. In the reaction catalyzed by carbon monoxide dehydrogenase/acetyl-coenzyme A synthase A, a channel between subunits

[†] This work was supported by National Institutes of Health Grants HL53306 (N.S.S.) and GM63262 (A.V.).

* To whom correspondence should be addressed. Phone: (631) 632-7952. Fax: (631) 632-5731. E-mail: nicole.sampson@stonybrook.edu.

[‡] Stony Brook University.

[§] University of California.

[||] University of Western Australia.

10.1021/bi800228w CCC: $40.75
Published on Web 04/15/2008

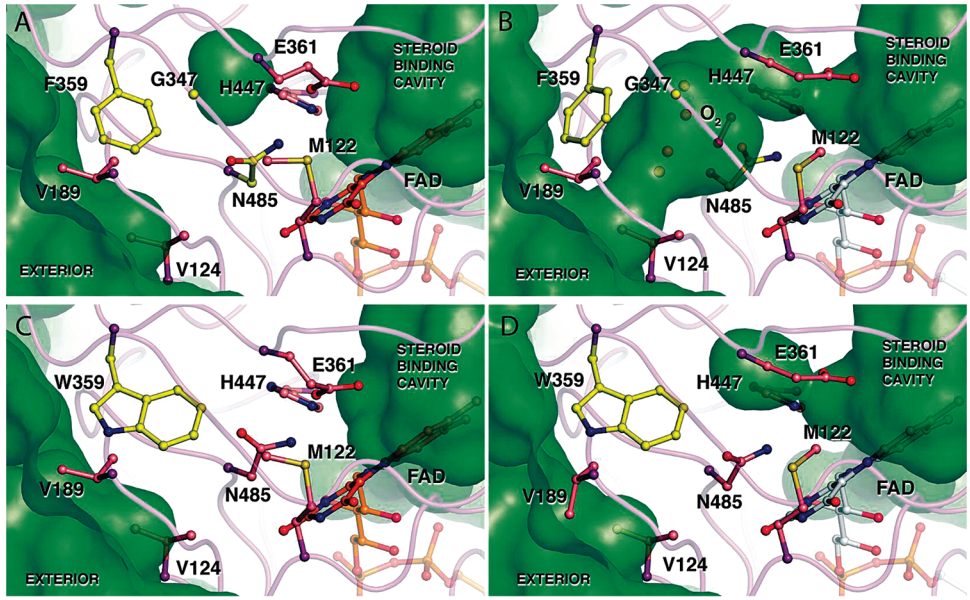

FIGURE 1: Atomic-resolution structure of (A and B) wild-type (1MXT) and (C and D) F359W (3CNJ) cholesterol oxidases with key residues in the proposed oxygen tunnel shown in their closed (A and C) and open (B and D) conformations. The solvent accessible surface calculated using a probe radius of 1.4 Å is colored green. The hydrophobic tunnel between the flavin and the exterior is present when the wild-type tunnel residues are in their open conformation (B) but blocked in the wild-type closed conformation (A). The open conformation includes a dioxygen species which was modeled in the tunnel with a fixed occupancy of 0.25 (*37*). However, the density may also represent two alternate water conformations. Inclusion in the model of either a dioxygen species or two alternate water molecules requires the adjacent active site and tunnel residues to be present in conformer B. Tryptophan 359 obstructs the tunnel in both conformations (C and D). However, the other tunnel residues, e.g., Glu361, Met122, and Val124, can adopt the closed (C) or open (D) conformation. Images were created using Pymol (*41*).

is proposed to allow transport of CO or CO_2 to the active site and between active sites (*11*). Mutation of amino acids to block this channel appears to block the access of CO and CO_2 to the active site (*12*). These enzymes are primarily multimeric and require a tunnel or channel to pass the intermediate from one subunit to the next.

Enzymes that utilize a gas as a substrate, as opposed to as an intermediate, have different mechanistic requirements. In these cases, the substrate is already present in the bulk solution and must reach the active site. Binding gaseous substrate through a tunnel allows temporal and regiocontrol of its reaction with a second substrate, thus conferring a mechanistic advantage. For example, soybean lipoxygenase generates an alkyl radical intermediate. If activated oxygen is not aimed at a specific carbon, many regioisomers could result. A channel has been proposed to act as a reservoir for O_2 that directs it through the protein to react predominantly at C-13 of the linoleyl radical (*13, 14*). Mutation of Ile553 to Phe in this channel reduces oxygen access (k_{cat}/K_{mO_2}) to the radical intermediate without altering the rate of other steps in the catalytic cycle. Similarly, a related channel has been shown to function identically in the rabbit lipoxygenase, although other tunnels may function less efficiently when the main tunnel is blocked by mutagenesis (*15*). The cyclooxygenase system is believed to behave similarly with oxygen channeling responsible for stereochemical control of peroxy radical formation to form the required regioisomer (*16*). However, in this system, reversible kinetic partitioning of the undesired peroxy radical intermediates also provides regiocontrol (*17*). In a well-studied family, the copper amine oxidases, the oxygen binding properties have been examined extensively by potential of mean force calculations and crystallography (*18, 19*). In this case, several distinct oxygen binding pathways were identified. On the basis of mutagenesis studies, it was concluded that multiple pathways are utilized to different extents, which is analogous to the observations in the rabbit lipoxygenase system (*15*). The classic example of a protein binding oxygen is that of heme proteins myoglobin and hemoglobin (*20*). Although these proteins are not enzymes, several low-affinity binding sites for oxygen (or CO) have been observed by crystallographic and spectroscopic methods (*1, 21*−*23*).

In other cases, tunnels have been observed in enzymes, but their role as gas access routes has not been functionally demonstrated. For example, 3-hydroxybenzoate hydroxylase has a hydrophobic tunnel that leads to a discrete binding pocket that is proposed to be the oxygen-binding site (*24*). The structure of L-amino acid oxidase in the presence of L-phenylalanine reveals a Y-shaped channel that may bind the substrate oxygen and release the product hydrogen peroxide (*25*). A hydrophobic tunnel proposed to bind oxygen and hydrogen peroxide is also present in the type II cholesterol oxidase (*26*). Hydrophobic channels that could bind hydrogen gas were observed in the xenon-saturated structure of Ni−Fe hydrogenase (*27*).

The atomic structure of type I cholesterol oxidase has been determined to 0.95 Å resolution (*28*). At this resolution, the two conformations of approximately 80 amino acid residues are resolved. In one conformation, several amino acids are oriented such that a narrow, hydrophobic tunnel extending from the outside surface of the enzyme to the buried active site is formed. In the alternate conformation, the tunnel is closed (Figure 1A,B). The orientation and size of this tunnel suggest that it provides a passageway for the access of oxygen to the active site and release of hydrogen peroxide to the aqueous solvent. Phe359, Val189, Val124, and Gly347 frame the entrance to the tunnel. At the other end of the

tunnel, Asn485 and Met122 form a gate between the tunnel and the isoalloxazine ring of the flavin. The tunnel is only long enough to house two oxygen molecules (Figure 1B).

Cholesterol oxidases are bacterial, monomeric flavoenzymes that catalyze the oxidation of cholesterol to cholest-5-en-3-one. The flavin dinucleotide cofactor is simultaneously reduced. The reduced flavin is in turn oxidized by oxygen with concomitant formation of hydrogen peroxide. The cholest-5-en-3-one that is formed is isomerized to cholest-4-en-3-one in the same active site. Cholest-5-en-3-one is susceptible to radical oxygenation and most likely is isomerized in situ to the more stable cholest-4-en-3-one to prevent this side reaction (*29*).

An amide$-\pi$ interaction between the side chain of Asn485 in cholesterol oxidase and the pyrimidine ring of the FAD[1] stabilizes the reduced flavin (*30*). When the substrate is oxidized and the FAD cofactor is reduced, the side chain of Asn485 rotates toward the cofactor and a series of conformational changes involving other tunnel residues are initiated. These conformational changes result in the tunnel open conformation, suggesting that the conformation of Asn485 and, by implication, the oxidation state of the flavin regulate access of oxygen to the active site from this tunnel.

Despite the structural observation of a tunnel in this enzyme, no functional evidence that there is a specific binding pathway, e.g., a tunnel, has been forthcoming. To test the functional importance of the tunnel, we investigated the effects of mutating tunnel residues, Phe359, Asn485, and Gly347. The kinetics of the reactions catalyzed by mutant cholesterol oxidases were interpreted with respect to the Phe359 mutant enzyme and wild-type atomic-resolution structures.

MATERIALS AND METHODS

General Materials and Methods. Water for assays and chromatography was distilled followed by passage through an 18 MΩ filtration system. A Shimadzu UV2501 PC spectrophotometer was used for kinetic assays and acquisition of UV spectra. Fluorescence measurements were taken with a Spex Fluorolog 3-21 spectrofluorometer. The following buffers were used: buffer A, 50 mM sodium phosphate (pH 7.0); buffer B, buffer A with 0.025% Triton X-100 (w/v); buffer C, buffer B with 0.01% BSA (w/v); and buffer D (10× HEPES), 1.37 M NaCl, 0.06 M D-(+)-glucose, 0.05 M KCl, 0.007 M $Na_2HPO_4 \cdot 7H_2O$, and 0.2 M HEPES (pH 7.1).

Construction of pCO303 and Other Mutant Expression Plasmids. A 214-base oligonucleotide was made by PCR using two primers. Primer 1 contained the designated mutation site and a *Mlu*I site (5′-CggCATCgACgCgTgggACAACAgCgACTCCTCggTCTgggCggAgATCgCCCCCATgCC-3′). Primer 2 corresponded to the anticoding strand and contained a *Hin*dIII site (5′-gCTCACAATTCCACACAA-3′). With these two primers and using *Xho*I-restricted pCO202 (*30*) as a template, 35 cycles of PCR were performed with iProof polymerase (Bio-Rad Laboratories, Hercules, CA) at an annealing temperature of 72 °C. The PCR fragment was digested with *Mlu*I and *Hin*dIII, purified, and subcloned into pCO200 (*31*) that had been similarly digested to yield F359W ChoA mutant expression plasmid pCO303. The N485D and G347N mutants were constructed in a similar fashion to yield plasmids pCO300 and pCO302 with the following primers and restriction sites: pCO300, 5′-ggCTggggCCCCAACggTAACATCATgACCgCCgggCCAACCACATgTggAACCCCACCggCgCCC-3′ (*Stu*I) and 5′-gCTCACAAgCTTACgACgCCgTgACgTCCTgCTTgATgATgCgCTCgACgTTCCgCTCggCCAgCgCCgTgATggTCACgAACgggAggACgCCgACgg-3′ (*Hin*dIII); pCO302, 5′-ggAACCCCACCggCgCCCACCAgTCCTCCATCCCCgCCCTCAATATCgACgCgTgggAC-3′ (*Sgr*AI) and 5′-GCTCACAATTCCACACAA-3′ (*Hin*dIII). Sequencing of these clones was conducted at the Stony Brook University sequencing facility using an ABI 3730 genetic analyzer (Applied Biosystems, Foster City, CA).

Protein Purification of Wild-Type and Mutant Cholesterol Oxidases. Wild-type and mutant cholesterol oxidases were purified as previously described (*30*). Fractions were assayed for content and purity by SDS−PAGE. Fractions containing pure cholesterol oxidase (>98%) were combined and ultrafiltered (YM30 membrane) into buffer A for storage.

Steady-State Kinetic Assays of Wild-Type and Mutant Cholesterol Oxidases. Solutions of cholesterol oxidase were prepared in buffer C. Stock solutions of steroids were prepared by dissolving the appropriate sterol in propan-2-ol. The initial velocities of wild-type and mutant cholesterol oxidases were measured in one of two ways. (1) The formation of conjugated enone was followed as a function of time at 240 nm ($\varepsilon_{240} = 12100\ M^{-1}\ cm^{-1}$). The detergent micelles were allowed to form at 37 °C for 10 min; cholesterol was added, and the solution was equilibrated for 10 min. The reaction was initiated by adding cholesterol oxidase (wild type or mutant). (2) The rate of H_2O_2 formation was determined using a horseradish peroxidase-coupled assay. The reaction was followed by excitation at 325 nm and by monitoring the fluorescence emission at 415 nm (1.5 nm slits) to quantitate the rate of formation of H_2O_2. The standard assay conditions were the same as those of the UV A_{240} assay with the addition of 1.0 mM *p*-hydroxyphenylacetic acid and 10 units of horseradish peroxidase.

Steady-state kinetics for two varied substrates were measured using the UV A_{240} assay except that the assay solution (buffer C and cholesterol) was equilibrated with mixtures of N_2 and O_2 to vary the concentration of oxygen. Different ratios of oxygen and nitrogen were generated using a two-gas mixer (Aalborg Corp., Orangeburg, NY). The assay solution was evacuated under high vacuum and purged with the appropriate gas mixture every 10 min over a period of 2 h. The oxygen concentration in the assay buffer was determined using an oxygen meter (YSI model 53, Yellow Springs Instruments, Yellow Springs, OH).

Independent sets of initial velocity data were globally fit to the following equations using Grafit (version 4.0.10). Primary isotope effects were determined by fitting all the possibilities and selecting the best fit (^DV, $^DV/K$, or ^DV and $^DV/K$).

Fixed second substrate Michaelis−Menten equation

$$v = (V_m^{app}[S])/(K_m^{app} + [S]) \quad (1)$$

[1] Abbreviations: chox, cholesterol oxidase; choA, *Streptomyces* cholesterol oxidase; LB, Luria broth; IPTG, isopropyl α-D-thiogalactoside; SDS−PAGE, sodium dodecyl sulfate−polyacrylamide gel electrophoresis; HRP, horseradish peroxidase; 2×YT, 2× yeast-tryptone broth; BSA, bovine serum albumin; GMC, glucose/methanol/choline; FAD, flavin adenine dinucleotide; KIE, kinetic isotope effects; HEPES, 4-(2-hydroxyethyl)-1-piperazineethanesulfonic acid.

^{D}V and $^{D}V/K$ kinetic isotope effect equation

$$v = V_m^{app}[S][1 + f_i(KIE - 1)]/(K_m^{app} + [S]) \quad (2)$$

Ternary complex Michaelis−Menten equation

$$v = (V_m[A][B])/(K_{ia}K_{mb} + K_{mb}[A] + K_{ma}[B] + [A][B]) \quad (3)$$

Kinetic cooperativity steady-state rate equation

$$v = V_m^{app}[S]^h/(K_m^{app})^h + [S]^h) \quad (4)$$

Secondary equations for the two-substrate, ternary complex reaction

$$V_m^{app} = V_m[chol]/(K_{mChol} + [chol]) \quad (5)$$

$$(V_m/K_{mO_2})^{app} = (V_m/K_{mO_2})[chol]/(K_{iO_2}K_{mChol}/K_{mO_2} + [chol]) \quad (6)$$

where K_{mO_2} and K_{mChol} are the Michaelis constants for oxygen and cholesterol at saturating concentrations of cholesterol and oxygen, respectively, K_{iO_2} is the dissociation constant for the enzyme and oxygen, V_m is the maximum velocity, V_m^{app} and K_m^{app} are the apparent rate constants for a varied substrate S at a fixed concentration of the second substrate, f_i is the fraction of the heavy isotope present, KIE is the kinetic isotope effect, and h is the Hill or cooperativity coefficient.

Reduction Potential Measurements. Potentiometric titrations were performed to determine the midpoint potential of wild-type and mutant cholesterol oxidases in a spectroelectrochemical cell using the method of Stankovich (*32, 33*). Methyl viologen (100 μM) was used as the mediator dye to transfer electrons from the electrode to the protein (30 μM) and the redox indicator dye (2−10 μM). For wild-type cholesterol oxidase, indigo disulfonate, 2-amino-1,4-naphthoquinone, and cresyl violet were used as redox indicator dyes. For N485D, riboflavin and phenosafranin were used, and for F359W, indigo disulfonate and cresyl violet were used as indicator dyes. Before each titration, the enzyme solutions in buffer A underwent 12 cycles of vacuum and Ar purging over 2 h. Then the electrodes (working, auxiliary, and reference electrodes) were inserted into the spectroelectrochemical cell under positive Ar pressure, and the titration was initiated by adding electrons from a potentiostat (model 800B, CH Instruments, Austin, TX). After each addition of electrons, the system was allowed to equilibrate at 25 °C for 30 min, and then a visible spectrum and the system potential were recorded. The redox indicator dyes were titrated under the same conditions. The enzyme titration data were corrected for the absorbance of the oxidized and reduced dye at each potential to obtain the spectra of enzyme alone. The potentials were measured with a Ag/AgCl electrode and corrected to the standard hydrogen electrode. The concentrations of all species of the enzyme were calculated from the spectra and the molar absorptivities and were plotted versus the equilibrium potential of the system using the Nernst equation (eq 7),

$$E_{cell} = E^{\circ\prime}_{enzyme} + 0.059 \log([ox]/[red]) \quad (7)$$

where E_{cell} is the measured cell potential, $E^{\circ\prime}_{enzyme}$ is the potential of the enzyme, and [ox] and [red] are the concentrations of oxidized and reduced enzyme species, respectively.

Crystallization, Data Collection, and Data Processing. The atomic-resolution crystal structure of the WT cholesterol oxidase (1MXT) was reported previously (*28, 34*). Crystals of the F359W mutant enzyme were obtained by the hanging drop vapor diffusion method in 15% polyethylene glycol (PEG) 8000, 75 mM $MnSO_4$, and 100 mM sodium cacodylate (pH 5.2). Growth of mutant enzyme crystals was stimulated by microseeding from crystals of the WT enzyme. Crystals suitable for data collection grew within 2 weeks.

X-ray diffraction data were collected at Stanford Synchrotron Radiation Laboratory (SSRL) beamline 9-2 in two sweeps. The first set was collected to the maximum resolution attainable, which in this case was 0.95 Å, while the second set was collected to a resolution of ~1.5 Å to minimize the number of overloaded reflections at lower resolutions. The two data sets were integrated individually and then scaled together using the d*Trek suite of software (*35*). Final data collection statistics are listed in Table 4.

The structure of the F359W mutant enzyme was determined by difference Fourier techniques, using a starting model adapted from the 0.95 Å structure of the wild-type enzyme (1MXT). This model was modified as follows. All anisotropic *B*-factor parameters were removed, and side chains for Asn485, Met122, Val124, Val191, Phe359, Leu377, His447, and Asp459 were changed to alanines. Finally, the FAD cofactor and all the solvent molecules (including water, glycerol, and SO_4) were removed. The starting model was subjected to a round of rigid body refinement using Refmac5 (*36*), after which the FAD molecule, many of the truncated side chains, and many of the best-coordinated water molecules became visible as difference electron density features and were modeled. Subsequently, several cycles of restrained refinement using isotropic temperature factors were carried out in Refmac5, followed by manual modeling of features emerging in improved electron density maps using Coot (*37*).

Thereafter, refinement was carried out using SHELXH (*38*) as described previously (*28, 34*). Briefly, anisotropic temperature factor parameters and alternate side chain conformations were gradually introduced at this time, resulting in a dramatic overall improvement in R values. Later in the refinement process, hydrogen atoms were modeled using the "riding model", where the hydrogen atom's position is fixed relative to the atom to which it is bonded. The final stage of refinement involved minor adjustments, mostly involving water molecules with partial occupancy. The structure was validated using SFCHECK (*39*) and PROCHECK (*39*) from the CCP4 suite of software (*40*). The final refinement statistics are reported in Table 4. All structure figures were generated using PyMOL (*41*). The structure of the F359W mutant cholesterol oxidase has been deposited in the Protein Data Bank as entry 3CNJ.

RESULTS

Construction and Purification of WT and Mutant Cholesterol Oxidases. The mutant cholesterol oxidase genes were constructed, and the corresponding proteins were heterologously expressed in *Escherichia coli* and purified as previously described for other mutants and the wild-type enzyme (*30*). The isolated proteins were determined to be greater than 99% pure by SDS−PAGE analysis and UV−vis spectroscopy.

Table 1: Assessment of the Impact of Mutation on Oxidation, Isomerization, and Steroid Binding by Measurement of Apparent Steady-State Michaelis−Menten Rate Constants for Cholesterol Turnover[a]

	substrate turnover,[b] H_2O_2 detection		substrate turnover,[b] cholest-4-en-3-one detection		intermediate turnover,[c] cholest-4-en-3-one detection	
enzyme	k_{cat}^{app} (s^{-1})	K_{mChol}^{app} (μM)	k_{cat}^{app} (s^{-1})	K_{mChol}^{app} (μM)	k_{cat}^{app} (s^{-1})	K_{m5EO}^{app} (μM)
wild type	47 ± 4	2.7 ± 0.3	42 ± 1	2.7 ± 0.3	61 ± 4	7 ± 1
F359W	1.3 ± 0.1	4 ± 1	0.86 ± 0.05	2.7 ± 0.8	23 ± 1	7 ± 1
G347N	0.85 ± 0.04	5 ± 1	1.0 ± 0.1	1.5 ± 0.6	12.0 ± 0.5	5.0 ± 0.8
N485D	$(35 \pm 4.4) \times 10^{-3}$	6.2 ± 2.2	$(73 \pm 5) \times 10^{-3}$	7 ± 1	10 ± 1	7.2 ± 0.9

[a] Initial velocity data were fit to the Michaelis−Menten equation for a single substrate (eq 1). Values reported are the means of three independent measurements, and errors are the standard deviation of the mean. [b] Cholesterol was used as a substrate at an ambient O_2 concentration of 256 μM. [c] Cholest-5-en-3-one was used as a substrate at an ambient O_2 concentration of 256 μM.

Kinetic Characterization of Tunnel Mutants. Using cholesterol as a substrate at a fixed O_2 concentration of 256 μM (buffer saturated with air), steady-state kinetic assays were used to initially characterize the wild-type and mutant cholesterol oxidases. Individual mutation of the tunnel residues reduced k_{cat}^{app} for substrate conversion 30−575-fold and had little effect on the K_{mChol}^{app} (Table 1).

Cholesterol oxidase catalyzes the oxidation of cholesterol to cholest-5-en-3-one followed by its isomerization to cholest-4-en-3-one. Two steady-state kinetic assays were used to elucidate the individual effect of the mutations on these two chemical steps. One assay follows the formation of product cholest-4-en-3-one, and the second assay follows the formation of product H_2O_2. If the isomerization reaction is slowed or cholest-5-en-3-one binding is weakened by mutation, the intermediate cholest-5-en-3-one is released before it is isomerized (*29*), and different rates will be measured by the two assays. Comparison of the rate constants from the two assays shows that the intermediate is not released by any of the mutants. Direct measurement of the rate of isomerization using the intermediate cholest-5-en-3-one as a substrate confirmed that isomerization is not perturbed more than 6-fold in k_{cat}^{app} by mutation (Table 1) and the K_m^{app} values for steroid are unaffected. Thus, reduced rates of steroid binding and release or a reduced rate of isomerization is not responsible for the 40−600-fold rate reductions caused by these mutations.

These data suggested mutation of the tunnel residues primarily affected the oxidation chemistry catalyzed by cholesterol oxidase. In the wild-type-catalyzed reaction, a primary kinetic isotope effect on hydride transfer from cholesterol to $FADH^-$ is observed on both k_{cat}^{app} and $(k_{cat}/K_{mChol})^{app}$, requiring that oxidation of cholesterol is at least partially rate limiting at both subsaturating and saturating cholesterol concentrations. The primary kinetic isotope effects on hydride transfer are greatly reduced in the cholesterol oxidation reactions catalyzed by all of the mutants except N485D (Table 2). The effects of mutation of asparagine 485 on catalytic efficiency are pleiotropic (*42, 43*). The majority of the rate reduction upon asparagine mutation is due to lessening the oxidation power of the flavin cofactor (*30, 42*). The midpoint potential of N485D is -211 ± 6 mV and is reduced 80 mV with respect to that of the wild-type enzyme. In contrast to N485D, the midpoint potential of F359W is reduced only 20 mV to -153 ± 4 mV. The combination of reduced catalytic activity in the redox step, reduced sensitivity to deuterium substitution, and marginally reduced rates of isomerization suggests that either oxygen binding or $FADH^-$ oxidation has become rate-limiting in the reactions catalyzed by the F359W and G347N mutants.

Table 2: Assessment of the Impact of Mutation on the Kinetic Isotope Effect for Hydride Transfer from Cholesterol to FAD by Measurement of Apparent Steady-State Michaelis−Menten Rate Constants for Cholesterol Turnover[a]

enzyme	^DV and $^DV/K$
wild type[b]	2.2 ± 0.1
F359W	1.2 ± 0.2
G347N	1.7 ± 0.2
N485D	2.5 ± 0.2

[a] Initial velocity data were measured for cholesterol or [3-^{2}H]cholesterol as a substrate at a fixed O_2 concentration of 256 μM and fit to eq 2 for the same isotope effect on k_{cat}^{app} (V) and $(k_{cat}/K_m)^{app}$ (V/K). Values reported are the means of three independent measurements, and errors are the standard deviation of the mean. [b] Taken from ref *30*.

Further steady-state assays were performed to identify the source of the rate decrease. The oxygen concentration was varied in addition to the cholesterol concentration, and the formation of product cholest-4-en-3-one was followed. The dependence of wild-type rate on varied oxygen concentration fit a classical hyperbolic saturation curve (Figure 2A), as did the dependence of rate on varied cholesterol. The combined oxygen and cholesterol data fit a model in which a ternary complex of steroid, oxygen, and enzyme is formed (Figure 2B). The data were inconsistent with a ping-pong model in which cholest-4-en-3-one, the first product, is released before binding of O_2, the second substrate.

The rate dependencies on oxygen concentration of the mutant-catalyzed reactions were strikingly different from those of the wild-type-catalyzed reaction. The N485D-catalyzed reaction was linearly dependent on oxygen concentration within the experimentally accessible range of oxygen concentrations (Figure 3A). In this concentration range, the reaction catalyzed by N485D is second-order, i.e., dependent on both oxygen and enzyme concentration, suggesting that the K_m for oxygen has been increased to a concentration above the solubility limit of oxygen in aqueous buffer. The F359W- and G347N-catalyzed reactions were sigmoidally dependent on oxygen concentration and were fit to the Hill equation for cooperativity (eq 4, Figure 3B,C, and Table 3). The Hill coefficient for the reaction catalyzed by F359W increased with increasing concentrations of cholesterol, and the maximal cooperativity coefficient was 1.8 ± 0.2 (Table 3). Although the reaction catalyzed by G347N appeared to be cooperative, the data could not be fit reliably because the K_m for O_2 is close to the aqueous solubility limit of oxygen. Therefore, these data were not analyzed further. Reanalysis of the data for the wild-type-

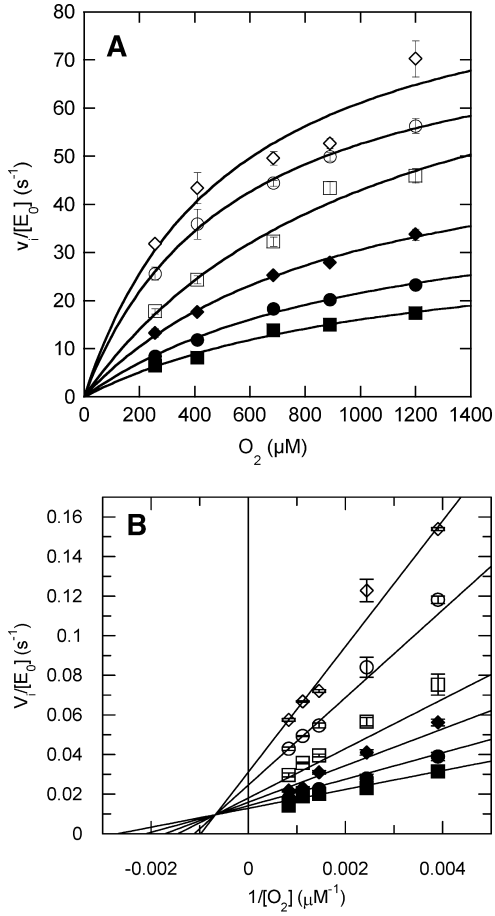

FIGURE 2: Steady-state kinetic profile of wild-type cholesterol oxidase. Initial velocities for wild-type cholesterol oxidase were measured over a range of O_2 concentrations with varied cholesterol concentrations. The data were globally fit to eq 3 for a sequential ternary mechanism, or they were fit to eq 4 for a cooperative mechanism at each individual cholesterol concentration. For the fit to eq 4, the Hill coefficient, h, was 1.0 at all cholesterol concentrations and the fit shown is for eq 3. The data shown are the averages of two independent experiments, and the errors are the standard deviation of measurement. (A) Michaelis−Menten plots for $v_i/[E_o]$ vs $[O_2]$ at varied cholesterol concentrations: (◇) 30, (○) 15, (□) 9, (◆) 6, (●) 3, and (■) 2 μM cholesterol. (B) Double-reciprocal plot of the data in panel A. The intersecting line pattern is consistent with the formation of a ternary complex among the enzyme, oxygen, and steroid.

catalyzed reaction utilizing the Hill equation confirmed that there was no apparent oxygen cooperativity in the wild-type-catalyzed reaction. The Hill coefficients at all cholesterol concentrations were 1; that is, the curves were hyperbolic, not sigmoidal (Figure 2A). The K_{mO_2} is increased 2-fold to 617 μM with the F359W mutation, and k_{cat} is decreased 13-fold relative to that of the wild type.

The kinetic cooperativity of the oxygen reaction was investigated with a poor substrate, dehydroepiandrosterone. In the wild-type-catalyzed reaction, k_{cat}^{app} is 20 times slower with dehydroepiandrosterone as a substrate than with cholesterol at an ambient oxygen concentration of 256 μM. The wild-type-catalyzed reaction has a hyperbolic dependence on oxygen concentration with a $K_{mO_2}^{app}$ of 342 ± 64 μM and a k_{cat}^{app} of 1.34 ± 0.09 s^{-1} (Figure 4). Importantly, the F359W-catalyzed reaction is not cooperative with respect to oxygen when dehydroepiandrosterone is utilized as the substrate. The F359W-catalyzed reaction also exhibits a hyperbolic dependence on oxygen concentration with a $K_{mO_2}^{app}$ of 544 ± 73 μM and a k_{cat}^{app} of 1.35 ± 0.08 s^{-1} (Figure 4). This result indicates that the kinetic cooperativity observed with cholesterol is lost

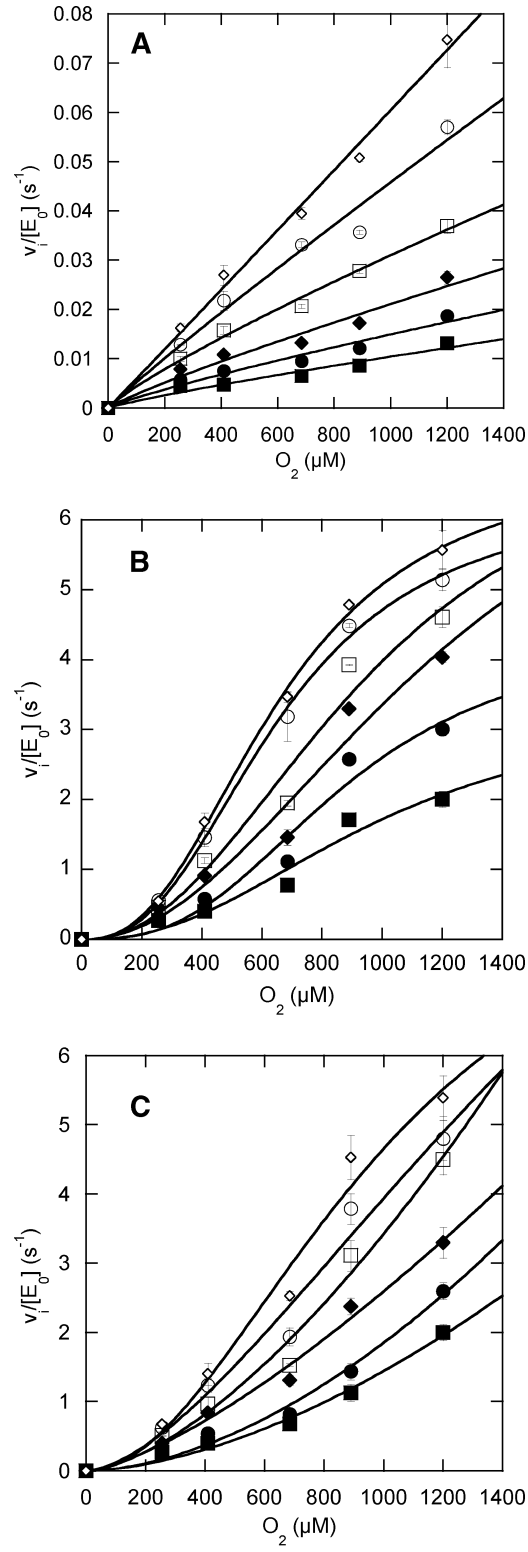

FIGURE 3: Steady-state kinetic profiles of mutant cholesterol oxidases. Initial velocities for mutant cholesterol oxidases were measured over a range of O_2 concentrations with varied cholesterol concentrations and the data fit to eq 4 for a cooperative mechanism at each individual cholesterol concentration: (◇) 30, (○) 15, (□) 9, (◆) 6, (●) 3, and (■) 2 μM cholesterol. (A) N485D, (B) F359W, and (C) G347N. The data shown are the averages of two independent experiments, and the errors are the standard deviation of measurement.

Table 3: Steady-State Rate Constants for Wild-Type and F359W Cholesterol Oxidases

enzyme	K_{iO_2} (μM)	K_{mO_2} (μM)	K_{mChol} (μM)	k_{cat} (s^{-1})	h_{max}	$(k_{cat}/K_{mO_2})^{wt}/(k_{cat}/K_{mO_2})^{mut}$	$(k_{cat}/K_{mChol})^{wt}/(k_{cat}/K_{mChol})^{mut}$
wild type[a]	1383 ± 120	300 ± 35	4.0 ± 0.5	96 ± 6	1.0[c]	1	1
F359W[b]	1381 ± 1649	617 ± 15	2.1 ± 2.5	7.4 ± 1	2.8[c]	27	6.8

[a] A compulsory order ternary complex mechanism as described in eq 3 was fit to the initial velocity data to yield K_{iO_2}, K_{mO_2}, and K_{mChol}. [b] Secondary plots of V_m^{app} and $(V_m/K_{mO_2})^{app}$ vs [cholesterol] were fit to eqs 5 and 6, respectively to yield V_m, K_{iO_2}, K_{mO_2}, and K_{mChol}. V_m^{app} and $(V_m/K_{mO_2})^{app}$ were obtained by fitting initial velocity data for varied oxygen concentrations at fixed cholesterol concentrations to eq 4. [c] h_{max} was determined by plotting h vs [cholesterol]. Values reported are the means of two independent measurements, and errors are the standard deviation of the mean.

Table 4: Crystallographic Data and Refinement Statistics for the F359W Cholesterol Oxidase Structure

Data Collection	
space group	$P2_1$
cell dimensions	
a, *b*, *c* (Å)	51.28, 72.87, 62.95
α, *β*, *γ* (deg)	90.0, 105.11, 90.0
resolution (Å)	46.7−0.95 (0.98−0.95)
no. of reflections (total)	1141795
no. of reflections (unique)	270322
R_{merge}	0.047 (0.48)
mean $I/\sigma(I)$	11.2 (1.9)
completeness (%)	96.3 (67.6)
redundancy	4.22 (2.56)
Refinement	
R_{work}/R_{free}	14.0/17.5
no. of atoms	
protein	4714
water	695
ligand/ion	63
isotropic *B*-factor	
protein (main chain)	12.11
protein (side chain)	15.52
FAD	8.4
rmsd	
bond lengths (Å)	0.013
bond angles (deg)	2.2
planarity (Å^3)	0.084
no. of alternate conformations	101

when the rate(s) of the kinetic step(s) subsequent to oxygen binding is reduced.

Atomic-Resolution Structure of the F359W Mutant. The crystal structure of the F359W mutant was refined to 0.95 Å resolution (Table 4). The mutant crystallizes in the same space group as the wild-type enzyme, and the overall structure of the mutant is the same. At this resolution in the wild-type structure, multiple conformations of amino acid residues were resolved into two distinct populations. In population A, the tunnel between solvent and active site is closed (Figure 1A). In population B, the tunnel residues are rotated out of the tunnel and an open passage is formed (*28*) (Figure 1B).

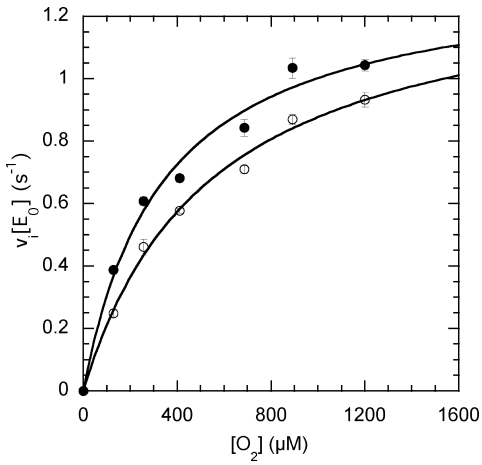

FIGURE 4: Initial velocities for wild-type and F359W cholesterol oxidases were measured over a range of O_2 concentrations with a fixed dehydroepiandrosterone concentration of 140 μM and fit to eq 1: (○) wild type and (●) F359W. The data shown are the averages of two independent experiments, and the errors are the standard deviation of measurement.

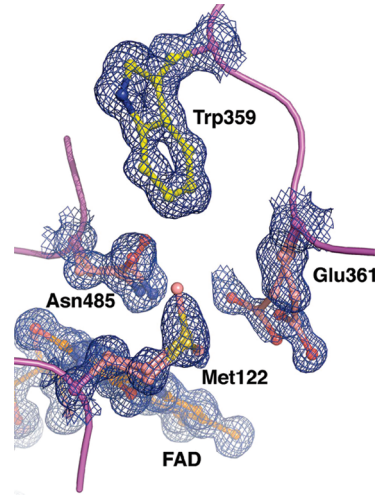

FIGURE 5: Electron density for a portion of the F359W active site, including Trp359. The density (blue mesh) was calculated using the coefficients $2F_o - F_c$ and contoured at 1.0σ. Alternate conformations for Glu361, Met122, and Asn485 could clearly be resolved, while no alternate conformations for Trp359 were observed.

In population A of the wild-type structure, the phenylalanine side chain fills the tunnel, and in population B, it undergoes an 18° rotation about χ_1 and the tunnel becomes solvent accessible. In the mutant structure, the indole ring of Trp359 is flipped into the tunnel in a position analogous to to the conformation of Phe359 in population A of the wild-type structure (Figures 1C,D and 5). A second conformation of Trp359 is not detected in the electron density maps (Figure 5), and as a result, no tunnel opening can be seen (Figure 1C,D). The conformations of the other tunnel residues as well as the active site residues differs little from those of the wild-type enzyme, with an rmsd of 0.144 Å between the two structures. The remaining residues that occupy two conformations in the wild-type structure also occupy two conformations in the F359W structure.

DISCUSSION

The mutation of phenylalanine 359 to tryptophan results in a 13-fold decrease in the rate of catalytic turnover. Importantly, the reduced mutant enzyme is still oxidized by oxygen with multiple catalytic cycles. The atomic-resolution structure of the mutant with a tryptophan at position 359 reveals the putative oxygen tunnel obstructed by the indole

Scheme 1: Mnemonic Model for the Kinetically Cooperative Oxygen Reaction in the Mutant-Catalyzed Reactions[a]

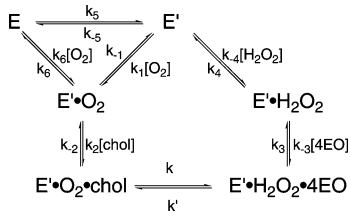

[a] Adapted from the work of Cornish-Bowden and Ricard (*44, 45*).

moiety. If the mutation blocked the tunnel to such an extent that oxygen can no longer traverse the tunnel and oxygen is forced to access the active site via the steroid-binding site, a ternary complex of oxygen and steroid would no longer be formed. The steroid-binding site is not sufficiently large to accommodate oxygen in addition to steroid. Kinetically, a ping-pong mechanism of substrate binding would be observed. That is, the steroid binding, conversion, and release would have to occur before oxygen binding and turnover. However, the kinetic profile of the F359W mutant, as well as those of the other two mutants (Figure 3 and Table 3), is inconsistent with this mechanism, and the model was not considered further.

The reactions catalyzed by the F359W and G347N mutants do not fit a classical ternary complex mechanism either. Instead, the mutations introduce positive cooperativity with respect to oxygen concentration. Cooperativity is generally associated with multisubunit proteins that relay binding occupancy and structural conformation information between subunits, for example, as occurs upon binding of oxygen to hemoglobin. Cholesterol oxidase is a monomeric enzyme, and thus, it is distinctly improbable that the cooperativity results from multisite binding of oxygen with successive changes in association constants and quaternary structure. The proposed wild-type gas-binding tunnel is large enough to accommodate two oxygen molecules. One could be bound as a substrate and the second as an allosteric effector. However, what remains of the tunnel in the F359W mutant is only large enough to accommodate half of one oxygen molecule (one water is observed in the electron density maps), and it is the mutant that shows positive cooperative behavior, not the wild-type enzyme. Furthermore, additional oxygen binding cavities were not observed in the mutant structure. Thus, a multisite binding model was not consistent with either the structural data or the wild-type kinetics.

Next, a kinetic cooperativity model was considered (*44, 45*). Monomeric enzymes display kinetic cooperativity under nonequilibrium conditions that are often due to a slow protein conformational change. In this model, two different protein conformations, E and E′, can bind O_2 followed by cholesterol to form a ternary complex, E′•O_2•cholesterol, and the ternary complex reacts to form products (Scheme 1). The reaction of E′ is faster than the reaction of E. The protein conformation E′ persists after product release, and at high oxygen concentrations, oxygen can bind to E′ before it has time to equilibrate to the more stable enzyme form, E. This kinetic trapping of E′ by O_2 occurs because the two conformations, E and E′, interconvert slowly and the rate of binding of O_2 is first-order in oxygen concentration. In this mechanism, the more active enzyme conformation, E′, appears to be remembered because it relaxes back to the E form so slowly and this type of kinetic cooperativity is known as mnemonic (*44, 45*). There are two consequences of this mechanism. The first consequence is that the reaction kinetics display cooperativity for only the first or preferred substrate, and no cooperativity for the second substrate. In the case presented here, there is no cooperativity with respect to cholesterol. The second consequence is that the positive cooperativity will increase with increasing concentrations of the second substrate. Again, this is the case for the F359W cholesterol oxidase.

The mnemonic model is consistent with both the F359W structure and kinetics. The tunnel is closed regardless of the conformation of the other tunnel residues (Figure 1C,D). As the passage of oxygen through the tunnel is sterically blocked by the mutation, it is assumed that oxygen must bind by another means, and this route is slower than the native binding mechanism through the tunnel. One possibility is diffusion through the protein by many different paths. After chemical conversion of cholesterol and O_2 to cholest-4-en-3-one and H_2O_2, respectively, the products are released. If the kinetic barrier to diffusion of H_2O_2 through the protein is much higher than the barrier to diffusion of H_2O_2 through the tunnel, the latter pathway will predominate. Alternatively, a second transient, and as yet undetected, pathway may open to release H_2O_2, which is postulated in the case of rabbit lipoxygenase (*15*). Upon H_2O_2 release, the exit path will be open. Because the open and closed tunnel conformations interconvert slowly and are not in equilibrium in the presence of high oxygen concentrations, oxygen can bind via the tunnel. This binding pathway is faster than diffusion through the protein, and cooperativity in time is observed. This mnemonic mechanism suggests that the F359W tunnel or an alternate pathway can be in an open conformation; however, this conformation is much higher in energy than the closed form, and the open−closed interconversion is kinetically slow.

The observation of a single tryptophan 359 conformation in the mutant structure suggests that the tryptophan conformation analogous to conformation B of phenylalanine 359 is not populated in the absence of substrate. In addition, rotation about χ_1 of tryptophan 359 cannot occur without simultaneous movement in the surrounding protein structure because unfavorable van der Waals contacts would occur during rotation. The increased steric bulk of the indole ring over that of a phenyl ring must destabilize conformation B and raise the barrier to its formation. The precise structure of the F359W tunnel open conformation is not known.

An alternative model is that in which oxygen binds only by diffusion through the protein and hydrogen peroxide is released only by diffusion. In this case, there is not a defined pathway of binding, but many paths would contribute to oxygen binding. If there were multiple accessible pathways, it would be very unlikely that the conformation of the enzyme (E′ in Scheme 1) released upon hydrogen peroxide exit would be in the optimal conformation for oxygen uptake, and kinetic cooperativity would not be observed upon mutation of Phe359 or Gly347.

We cannot completely exclude an alternative mechanism in which the substrates bind in random order, and the flux through the oxygen binding first pathway versus the cholesterol binding first pathway shifts upon with a change in

oxygen concentration (*46, 47*). This mechanism requires that substrate binding not be at equilibrium; that is, steps subsequent to ternary complex formation are fast relative to substrate binding. The implication that results is that mutation of tunnel residues slows oxygen binding, and our conclusions about the importance of a protein tunnel through which oxygen binds are unchanged.

The hydrophobic tunnel in cholesterol oxidase, as well as other oxidases, might be functionally most important when used as an exit for hydrogen peroxide. Upon reaction of hydrogen peroxide with amino acid side chains, the enzyme structures could be altered in ways deleterious to catalytic activity. It is possible that hydrophobic tunnels evolved to prevent the reactivity of the product from damaging the enzyme. Despite the relative hydrophilicity of hydrogen peroxide, a hydrophobic tunnel that lacked easily oxidized heteroatoms would be less susceptible to oxidative damage than a polar tunnel. In addition, channeling of oxygen to the reduced flavin via a tunnel would limit the peroxidation of the susceptible cholest-5-en-3-one intermediate.

The rest of the glucose/methanol/choline (GMC) oxidoreductase superfamily was surveyed for the presence of tunnel features in each of the structures. Few tunnel residues are conserved in the structure-based alignments except Phe359 from cholesterol oxidase. Other non-GMC oxidoreductases have tunnels that connect the protein surface to the active site, e.g., D-amino acid oxidase (*48*), *Hansenula polymorpha* copper-containing amine oxidase (*18*), and type II cholesterol oxidase (*26*). The conserved features are conformational flexibility, which is a feature not readily identified through sequence or structure alignments, and hydrophobicity, which can be satisfied by many constellations of hydrophobic amino acids. The multiplicity of solutions among oxidoreductases is similar to the structural diversity seen for ammonia transfer tunnels in different carbamoylphosphate synthetases (*49*) and oxygen tunnels in lipoxygenases (*15, 16*).

In addition, kinetic cooperativity has been observed in the steady-state reaction catalyzed by another glucose/methanol/choline oxidoreductase family member. Mutation of valine 464 in choline oxidase results in two conformers of the enzyme that slowly interconvert (S. Finnegan and G. Gadda, personal communication). The carbonyl of valine 464 forms a hydrogen bond to N5 of the flavin in the native enzyme structure (*50*), and thus, it could act as a sensor of flavin oxidation state to gate oxygen access. Although a tunnel is not observed in the native structure, this may be due to the presence of a flavin adduct in the active site that would preclude a tunnel opening conformational change by asparagine 510, the ortholog of asparagine 485 in cholesterol oxidase that appears to gate the conformation of other tunnel residues.

In conclusion, hydrophobic tunnels have been observed in many other protein structures, and their function as gas-binding tunnels has been hypothesized. The mutagenesis of three tunnel residues and their kinetic and structural characterization presented here provide functional evidence for the utility of the hydrophobic tunnel that spans ~18 Å between the solvent accessible surface and the active site of cholesterol oxidase. This tunnel provides oxygen access to the enzyme active site and, in the reverse direction, hydrogen peroxide access to solvent. That is, there is a specific binding pathway for oxygen to reach the reduced flavin cofactor and for hydrogen peroxide release. Our observations are in accordance with the observations of functional oxygen binding tunnels in the lipoxygenases (*15*). Similar tunnels observed in other protein structures are likely to function in a similar fashion. Their evolutionary selection is presumably derived from the need for temporal control as well as regiospecific control over oxygen delivery to reactive intermediates in enzyme-catalyzed reactions and protection of the enzyme from reactive products like hydrogen peroxide.

REFERENCES

1. Tilton, R. F., Jr., Kuntz, I. D., Jr., and Petsko, G. A. (1984) Cavities in proteins: Structure of a metmyoglobin-xenon complex solved to 1.9 Å. *Biochemistry 23*, 2849–2857.
2. Whittington, D. A., Rosenzweig, A. C., Frederick, C. A., and Lippard, S. J. (2001) Xenon and halogenated alkanes track putative substrate binding cavities in the soluble methane monooxygenase hydroxylase. *Biochemistry 40*, 3476–3482.
3. Duff, A. P., Trambaiolo, D. M., Cohen, A. E., Ellis, P. J., Juda, G. A., Shepard, E. M., Langley, D. B., Dooley, D. M., Freeman, H. C., and Guss, J. M. (2004) Using xenon as a probe for dioxygen-binding sites in copper amine oxidases. *J. Mol. Biol. 344*, 599–607.
4. de Sanctis, D., Dewilde, S., Pesce, A., Moens, L., Ascenzi, P., Hankeln, T., Burmester, T., and Bolognesi, M. (2004) Mapping protein matrix cavities in human cytoglobin through Xe atom binding. *Biochem. Biophys. Res. Commun. 316*, 1217–1221.
5. Raushel, F. M., Thoden, J. B., and Holden, H. M. (2003) Enzymes with molecular tunnels. *Acc. Chem. Res. 36*, 539–548.
6. Hyde, C. C., Ahmed, S. A., Padlan, E. A., Miles, E. W., and Davies, D. R. (1988) Three-dimensional structure of the tryptophan synthase $\alpha 2\beta 2$ multienzyme complex from *Salmonella typhimurium*. *J. Biol. Chem. 263*, 17857–17871.
7. Huang, X., and Raushel, F. M. (2000) Restricted passage of reaction intermediates through the ammonia tunnel of carbamoyl phosphate synthetase. *J. Biol. Chem. 275*, 26233–26240.
8. Raushel, F. M., Thoden, J. B., and Holden, H. M. (1999) The amidotransferase family of enzymes: Molecular machines for the production and delivery of ammonia. *Biochemistry 38*, 7891–7899.
9. Fan, Y., Lund, L., Yang, L., Raushel, F. M., and Gao, Y.-Q. (2008) Mechanism for the transport of ammonia within carbamoyl phosphate synthetase determined by molecular dynamics simulations. *Biochemistry 47*, 2935–2944.
10. Manjasetty, B. A., Powlowski, J., and Vrielink, A. (2003) Crystal structure of a bifunctional aldolase-dehydrogenase: Sequestering a reactive and volatile intermediate. *Proc. Natl. Acad. Sci. U.S.A. 100*, 6992–6997.
11. Volbeda, A., and Fontecilla-Camps, J. C. (2004) Crystallographic evidence for a CO/CO_2 tunnel gating mechanism in the bifunctional carbon monoxide dehydrogenase/acetyl coenzyme A synthase from *Moorella thermoacetica*. *J. Biol. Inorg. Chem. 9*, 525–532.
12. Tan, X., Volbeda, A., Fontecilla-Camps, J. C., and Lindahl, P. A. (2006) Function of the tunnel in acetylcoenzyme A synthase/carbon monoxide dehydrogenase. *J. Biol. Inorg. Chem. 11*, 371–378.
13. Knapp, M. J., and Klinman, J. P. (2003) Kinetic studies of oxygen reactivity in soybean lipoxygenase-1. *Biochemistry 42*, 11466–11475.
14. Knapp, M. J., Seebeck, F. P., and Klinman, J. P. (2001) Steric control of oxygenation regiochemistry in soybean lipoxygenase-1. *J. Am. Chem. Soc. 123*, 2931–2932.
15. Saam, J., Ivanov, I., Walther, M., Holzhutter, H. G., and Kuhn, H. (2007) Molecular dioxygen enters the active site of 12/15-lipoxygenase via dynamic oxygen access channels. *Proc. Natl. Acad. Sci. U.S.A. 104*, 13319–13324.
16. Furse, K. E., Pratt, D. A., Schneider, C., Brash, A. R., Porter, N. A., and Lybrand, T. P. (2006) Molecular dynamics simulations of arachidonic acid-derived pentadienyl radical intermediate complexes with COX-1 and COX-2: Insights into oxygenation regio- and stereoselectivity. *Biochemistry 45*, 3206–3218.
17. Mukherjee, A., Brinkley, D. W., Chang, K. M., and Roth, J. P. (2007) Molecular oxygen dependent steps in fatty acid oxidation by cyclooxygenase-1. *Biochemistry 46*, 3975–3989.
18. Johnson, B. J., Cohen, J., Welford, R. W., Pearson, A. R., Schulten, K., Klinman, J. P., and Wilmot, C. M. (2007) Exploring molecular

oxygen pathways in *Hansenula polymorpha* copper-containing amine oxidase. *J. Biol. Chem. 282*, 17767–17776.
19. Wilce, M. C. J., Dooley, D. M., Freeman, H. C., Guss, J. M., Matsunami, H., McIntire, W. S., Ruggiero, C. E., Tanizawa, K., and Yamaguchi, H. (1997) Crystal structures of the copper-containing amine oxidase from *Arthrobacter globiformis* in the holo and apo forms: Implications for the biogenesis of topaquinone. *Biochemistry 36*, 16116–16133.
20. Mims, M. P., Porras, A. G., Olson, J. S., Noble, R. W., and Peterson, J. A. (1983) Ligand binding to heme proteins. An evaluation of distal effects. *J. Biol. Chem. 258*, 14219–14232.
21. Ostermann, A., Waschipky, R., Parak, F. G., and Nienhaus, G. U. (2000) Ligand binding and conformational motions in myoglobin. *Nature 404*, 205–208.
22. Schmidt, M., Nienhaus, K., Pahl, R., Krasselt, A., Anderson, S., Parak, F., Nienhaus, G. U., and Srajer, V. (2005) Ligand migration pathway and protein dynamics in myoglobin: A time-resolved crystallographic study on L29W MbCO. *Proc. Natl. Acad. Sci. U.S.A. 102*, 11704–11709.
23. Scott, E. E., and Gibson, Q. H. (1997) Ligand migration in sperm whale myoglobin. *Biochemistry 36*, 11909–11917.
24. Hiromoto, T., Fujiwara, S., Hosokawa, K., and Yamaguchi, H. (2006) Crystal structure of 3-hydroxybenzoate hydroxylase from *Comamonas testosteroni* has a large tunnel for substrate and oxygen access to the active site. *J. Mol. Biol. 364*, 878–896.
25. Moustafa, I. M., Foster, S., Lyubimov, A. Y., and Vrielink, A. (2006) Crystal structure of LAAO from *Calloselasma rhodostoma* with an L-phenylalanine substrate: Insights into structure and mechanism. *J. Mol. Biol. 364*, 991–1002.
26. Coulombe, R., Yue, K. Q., Ghisla, S., and Vrielink, A. (2001) Oxygen access to the active site of cholesterol oxidase through a narrow channel is gated by an Arg-Glu pair. *J. Biol. Chem. 276*, 30435–30441.
27. Montet, Y., Amara, P., Volbeda, A., Vernede, X., Hatchikian, E. C., Field, M. J., Frey, M., and Fontecilla-Camps, J. C. (1997) Gas access to the active site of Ni-Fe hydrogenases probed by X-ray crystallography and molecular dynamics. *Nat. Struct. Biol. 4*, 523–526.
28. Lario, P., Sampson, N. S., and Vrielink, A. (2003) Sub-atomic resolution crystal structure of cholesterol oxidase: What atomic resolution crystallography reveals about enzyme mechanism and the role of the FAD cofactor in redox activity. *J. Mol. Biol. 326*, 1635–1650.
29. Sampson, N. S., and Kass, I. J. (1997) Isomerization, but not oxidation, is suppressed by a single point mutation, E361Q, in the reaction catalyzed by cholesterol oxidase. *J. Am. Chem. Soc. 119*, 855–862.
30. Ye, Y., Lario, P., Vrielink, A., and Sampson, N. S. (2001) The presence of a hydrogen bond betwen asparagine 485 and the π system of FAD modulates the redox potential in the reaction catalyzed by cholesterol oxidase. *Biochemistry 40*, 13779–13787.
31. Kass, I. J., and Sampson, N. S. (1998) The importance of Glu 361 position in the reaction catalyzed by cholesterol oxidase. *Bioorg. Med. Chem. Lett. 8*, 2663–2668.
32. Stankovich, M. T. (1980) An anaerobic spectroelectrochemical cell for studying the spectral and redox properties of flavoproteins. *Anal. Biochem. 109*, 295–308.
33. Stankovich, M. (2002) Potentiometric Measurements of Proteins, *Bioelectrochemistry* (Wilson, G. S., Ed.) pp 487−509, Wiley-VCH, Weinheim, Germany.
34. Lyubimov, A. Y., Lario, P. I., Moustafa, I., and Vrielink, A. (2006) Atomic resolution crystallography reveals how changes in pH shape the protein microenvironment. *Nat. Chem. Biol. 2*, 259–264.
35. Pflugrath, J. W. (1999) The finer things in X-ray diffraction data collection. *Acta Crystallogr. D55*, 1718–1725.
36. Murshudov, G. N., Vagin, A. A., and Dodson, E. J. (1997) Refinement of macromolecular structures by the maximum-likelihood method. *Acta Crystallogr. D53*, 240–255.
37. Emsley, P., and Cowtan, K. (2004) Coot: Model-building tools for molecular graphics. *Acta Crystallogr. D60*, 2126–2132.
38. Sheldrick, G. M., and Schneider, T. R. (1997) SHELXL: High-resolution refinement, *Methods in Enzymology* (Carter, C. W. J., and Sweet, R. M., Eds.) pp 319−343, Academic Press, Boston.
39. Vaguine, A. A., Richelle, J., and Wodak, S. J. (1999) SFCHECK: A unified set of procedures for evaluating the quality of macromolecular structure-factor data and their agreement with the atomic model. *Acta Crystallogr. D55*, 191–205.
40. Project, C. C. (1994) The CCP4 suite: Programs for protein crystallography. *Acta Crystallogr. D50*, 760–763.
41. DeLano, W. L. (2006) The PyMOL Molecular Graphics System, DeLano Scientific, San Carlos, CA.
42. Chen, L. (2007) The binding and release of oxygen and hydrogen peroxide are directed through a hydrophobic tunnel in cholesterol oxidase. Ph.D. Thesis, Department of Chemistry, Stony Brook University, Stony Brook, NY.
43. Lyubimov, A. (2006) A structural study of cholesterol oxidase at atomic and subatomic resoultion. Ph.D. Thesis, Department of Chemistry, University of California, Santa Cruz, CA.
44. Cornish-Bowden, A., and Cardenas, M. L. (1987) Co-operativity in monomeric enzymes. *J. Theor. Biol. 124*, 1–23.
45. Ricard, J., and Cornish-Bowden, A. (1987) Co-operative and allosteric enzymes: 20 years on. *Eur. J. Biochem. 166*, 255–272.
46. Pettersson, G. (1986) Mechanistic origin of the sigmoidal rate behaviour of glucokinase. *Biochem. J. 233*, 347–350.
47. Pettersson, G. (1986) Mechanistic origin of the kinetic cooperativity of hexokinase type L1 from wheat germ. *Eur. J. Biochem. 154*, 167–170.
48. Umhau, S., Pollegioni, L., Molla, G., Diederichs, K., Welte, W., Pilone, M. S., and Ghisla, S. (2000) The X-ray structure of D-amino acid oxidase at very high resolution identifies the chemical mechanism of flavin-dependent substrate dehydrogenation. *Proc. Natl. Acad. Sci. U.S.A. 97*, 12463–12468.
49. Weeks, A., Lund, L., and Raushel, F. M. (2006) Tunneling of intermediates in enzyme-catalyzed reactions. *Curr. Opin. Chem. Biol. 10*, 465–472.
50. Quaye, O., Lountos, G. T., Fan, F., Orville, A. M., and Gadda, G. (2008) Role of Glu312 in binding and positioning of the substrate for the hydride transfer reaction in choline oxidase. *Biochemistry 47*, 243–256.

BI800228W